

# Coupling of pairing and triaxial shape vibrations in collective states of $\gamma$ -soft nuclei

K. Nomura,<sup>1</sup> D. Vretenar,<sup>1,2</sup> Z. P. Li,<sup>3</sup> and J. Xiang<sup>4,3</sup>

<sup>1</sup>*Department of Physics, Faculty of Science, University of Zagreb, HR-10000 Zagreb, Croatia\**

<sup>2</sup>*State Key Laboratory of Nuclear Physics and Technology,*

*School of Physics, Peking University, Beijing 100871, China*

<sup>3</sup>*School of Physical Science and Technology, Southwest University, Chongqing 400715, China*

<sup>4</sup>*School of Physics and Electronic, Qiannan Normal University for Nationalities, Duyun 558000, China*

(Dated: May 26, 2021)

In addition to shape oscillations, low-energy excitation spectra of deformed nuclei are also influenced by pairing vibrations. The simultaneous description of these collective modes and their coupling has been a long-standing problem in nuclear structure theory. Here we address the problem in terms of self-consistent mean-field calculations of collective deformation energy surfaces, and the framework of the interacting boson approximation. In addition to quadrupole shape vibrations and rotations, the explicit coupling to pairing vibrations is taken into account by a boson-number non-conserving Hamiltonian, specified by a choice of a universal density functional and pairing interaction. An illustrative calculation for  $^{128}\text{Xe}$  and  $^{130}\text{Xe}$  shows the importance of dynamical pairing degrees of freedom, especially for structures built on low-energy  $0^+$  excited states, in  $\gamma$ -soft and triaxial nuclei.

## I. INTRODUCTION

An accurate description of the structure of deformed nuclei that cannot be characterized by axially symmetric shapes presents a challenge for low-energy nuclear theory [1, 2]. Quadrupole shape deformations, in particular, can be described in terms of the polar variables  $\beta$  and  $\gamma$ . The axial variable  $\beta$  is proportional to the intrinsic quadrupole moment, and the angular variable  $0 < \gamma < \pi/3$  specifies the degree of triaxiality. Two limiting cases for non-axial nuclei correspond to: (i) a collective potential with a stable minimum at a particular value of  $\gamma$  (the rigid-triaxial rotor model of Davydov and Filippov [3]) and, (ii) a collective potential that is virtually independent of the angular variable (the  $\gamma$ -unstable rotor model of Wilets and Jean [4]). Numerous studies of the emergence of  $\gamma$ -softness have shown that neither of the two limiting geometrical pictures is realized in actual nuclei. Most non-axial medium-heavy and heavy nuclei lie in between the limits of rigid-triaxiality and  $\gamma$ -unstable rotors [5–9].

An additional level of complexity is introduced by considering dynamical pairing in addition to shape collective degrees of freedom [10–14]. The interplay between pairing and triaxial quadrupole deformations has been a central subject in nuclear structure since the 1960s [15–18]. The effect of coupling between shape and pairing vibrations is evident in the excitation spectra, especially in the energies of bands based on excited  $0^+$  states, and the  $E0$  transition strengths [1, 19–23]. The dynamical pairing degree of freedom has been taken into account schematically in a number of studies that, however, did not explicitly consider the coupling between shape and pairing vibrations (see, for instances, Refs. [24–26]). In

two recent articles we have extended the quadrupole collective Hamiltonian [27], and the interacting boson model (IBM) [28], to include pairing vibrations and the coupling between shape and pairing degrees of freedom. It has been shown that the coupling to pairing vibrations produces low-energy spectra in much better agreement with experimental results. Both studies, however, have been restricted to axially symmetric shapes. As noted in Ref. [27], the effect of pairing vibrations will particularly be important for  $\gamma$ -soft nuclei characterized by shape coexistence [29] and, therefore, it is important to develop a model that allows for the coupling between pairing and triaxial  $(\beta, \gamma)$  shape degrees of freedom. In this work we develop such a model based on nuclear density functional theory and the IBM, and report the first microscopic calculation of pairing and triaxial shape vibrations in collective states of  $\gamma$ -soft nuclei.

## II. METHOD

To map the energy of a nucleus as function of intrinsic deformations, constrained self-consistent mean-field (SCMF) calculations [2, 30–33] are performed for a specific choice of the universal energy density functional and pairing force. In this work we employ the self-consistent relativistic mean-field plus BCS (RMF+BCS) model [34], based on the density functional PC-PK1 [35] and a separable pairing interaction [36]. The constraints imposed in the present SCMF calculation are the expectation values of the quadrupole moments  $\hat{Q}_{20}$  and  $\hat{Q}_{22}$ , and the monopole pairing operator  $\hat{P}$ . The expectation values of  $\hat{Q}_{20} = 2z^2 - x^2 - y^2$  and  $\hat{Q}_{22} = x^2 - y^2$  determine the deformation parameters  $\beta$  and  $\gamma$ , respectively. The expectation value of the monopole pairing operator  $\hat{P} = 1/2 \sum_{k>0} (c_k c_{\bar{k}} + c_{\bar{k}}^\dagger c_k^\dagger)$  in a BCS state, where  $k$  and  $\bar{k}$  denote the single-nucleon and the corresponding time-reversed states, respectively, defines the intrinsic pairing

\* knomura@phy.hr

deformation parameter  $\alpha$ , which can be related to the pairing gap  $\Delta$ . To reduce the computational complexity, no distinction is made between proton and neutron pairing degrees of freedom even though, in principle, they should be treated separately.

The three-dimensional potential energy surfaces (PES) of  $^{128}\text{Xe}$  and  $^{130}\text{Xe}$ , obtained in the  $(\alpha, \beta, \gamma)$ -constrained microscopic SCMF calculation, are projected onto two-dimensional planes in the first and third column of Fig. 1, respectively. The PESs are plotted as functions of the axial quadrupole and triaxial  $(\beta, \gamma)$ , axial quadrupole and pairing  $(\beta, \alpha)$ , and triaxial quadrupole and pairing  $(\gamma, \alpha)$  deformations. The fixed values of  $\alpha = 10$  (12) in the  $(\beta, \gamma)$  plot,  $\gamma = 18^\circ$  ( $0^\circ$ ) for the  $(\beta, \alpha)$  surface and, finally,  $\beta = 0.2$  (0.15) in the  $(\gamma, \alpha)$  map, correspond to the global minimum in the entire  $(\alpha, \beta, \gamma)$  parameter space of  $^{128}\text{Xe}$  ( $^{130}\text{Xe}$ ). While both nuclei appear to be  $\gamma$ -soft (first row of Fig. 1), the SCMF- $(\beta, \gamma)$  PES of  $^{128}\text{Xe}$  actually displays a shallow triaxial minimum at  $\gamma = 18^\circ$ . For  $\gamma = 18^\circ$  ( $0^\circ$ ), the  $(\alpha, \beta)$  surfaces of  $^{128}\text{Xe}$  ( $^{130}\text{Xe}$ ) exhibit shallow minima at  $\alpha = 10$  (12), respectively, and are rather soft with respect to the intrinsic pairing deformation parameter. As one can already infer from the first two maps, the  $(\gamma, \alpha)$ - energy surfaces at the minimum  $\beta$  are soft with respect to both collective coordinates. Softness, of course, implies large fluctuations and, therefore, both the triaxial  $\gamma$  and pairing  $\alpha$  degrees of freedom will be important for spectroscopic properties of these two nuclei.

To calculate excitation spectra and transition rates, one must extend the mean-field framework to include dynamical correlations that arise from restoration of broken symmetries and fluctuations of collective coordinates [2]. Physical quantities determined by collective dynamics are here computed by mapping the SCMF results onto a system of interacting bosons [37]. The boson model space consists of the monopole  $s$  and quadrupole  $d$  bosons that are associated with correlated  $J = 0^+$  and  $2^+$  pairs of valence nucleons, respectively. To take into account pairing vibrations, the number of bosons  $n_0$  which, by construction equals half the number of valence nucleons [38], is not conserved. Here we use a model with a Hilbert space expressed as a direct sum of three subspaces comprising  $n = n_0 - 1$ ,  $n_0$ , and  $n_0 + 1$  bosons:

$$(sd)^{n_0-1} \oplus (sd)^{n_0} \oplus (sd)^{n_0+1}. \quad (1)$$

The IBM Hamiltonian in general consists of boson-number conserving  $\hat{H}_{\text{cons}}$  and non-conserving  $\hat{H}_{\text{non-cons}}$  interactions:

$$\hat{H}_{\text{IBM}} = \hat{H}_{\text{cons}} + \hat{H}_{\text{non-cons}}. \quad (2)$$

For a quantitative description of  $\gamma$ -soft nuclei, the Hamiltonian must include not only one- and two-body boson terms, but also three-body terms [5, 8, 39–41]. It has been shown that already a minimal choice for a three-body boson interaction of the type  $(d^\dagger d^\dagger d^\dagger)^{(3)} \cdot (\tilde{d}\tilde{d}\tilde{d})^{(3)}$ , produces a triaxial minimum on the deformation energy

surface and provides a correct description of the structure of  $\gamma$ -bands [5, 8, 40, 41]. The boson number non-conserving Hamiltonian  $\hat{H}_{\text{non-cons}}$  is expressed in terms of a monopole pair-transfer operator  $(s^\dagger + s)$ , that either adds or removes an  $s$  boson [28].

The bosonic PES in the  $(\alpha, \beta, \gamma)$  space is computed by taking the expectation value of the IBM Hamiltonian in the boson condensate state  $|\Psi(\vec{\alpha})\rangle$  [42, 43]:

$$|\Psi(\vec{\alpha})\rangle = |\Psi_{n_0-1}(\vec{\alpha})\rangle \oplus |\Psi_{n_0}(\vec{\alpha})\rangle \oplus |\Psi_{n_0+1}(\vec{\alpha})\rangle, \quad (3)$$

where, for a given subspace comprising  $n$  bosons ( $n = n_0 - 1, n_0, n_0 + 1$ ),  $|\Psi_n(\vec{\alpha})\rangle$  is defined by

$$|\Psi_n(\vec{\alpha})\rangle = \left[ \alpha_s s^\dagger + \sum_{m=-2}^{+2} \alpha_m d_m^\dagger \right]^n |0\rangle, \quad (4)$$

up to a normalization factor. The vector  $\vec{\alpha}$  denotes the amplitudes  $\alpha_s$  and  $\alpha_m$ , and  $|0\rangle$  is the boson vacuum. The bosonic energy surface is expressed as a  $3 \times 3$  matrix  $\mathbf{E}(\vec{\alpha})$  [44]:

$$E_{n,n'}(\vec{\alpha}) = \langle \Psi_n(\vec{\alpha}) | \hat{H}_{\text{cons}} | \Psi_n(\vec{\alpha}) \rangle \delta_{n,n'} + \langle \Psi_{n'}(\vec{\alpha}) | \hat{H}_{\text{non-cons}} | \Psi_n(\vec{\alpha}) \rangle \delta_{n,n' \pm 1}, \quad (5)$$

with the three indices  $n_0$  and  $n_0 \pm 1$ .

The amplitudes  $\alpha_s$  and  $\alpha_m$  in 4 can be related to the pairing and triaxial deformation parameters of the SCMF calculations, respectively [28]. The boson Hamiltonian (2) is determined using the method of Ref. [28]. The parameters of the boson number conserving Hamiltonian  $\hat{H}_{\text{cons}}$  are specified by mapping the  $(\beta, \gamma)$ -SCMF PES at  $\alpha = \alpha_{\text{min}}$  onto the diagonal matrix element  $E_{n_0, n_0}(\alpha = \alpha_{\text{min}}, \beta, \gamma)$ . We note that only the strength of the rotational term  $\hat{L} \cdot \hat{L}$  in  $\hat{H}_{\text{cons}}$  is determined separately [45], by adjusting the moment of inertia of the yrast band to the empirical value. For  $^{128,130}\text{Xe}$  this value is  $\approx 40\%$  larger than the corresponding Inglis-Belyaev value [46, 47], computed using the SCMF single-nucleon quasiparticle states at the equilibrium minimum. The strength parameter of the number non-conserving Hamiltonian  $\hat{H}_{\text{non-cons}}$  is chosen in such a way that the  $(\alpha, \beta)$ -SCMF PES at  $\gamma = \gamma_{\text{min}}$  is reproduced by the lowest eigenvalue of the matrix  $\mathbf{E}(\vec{\alpha})$ . The details of the formalism for the 2D space  $(\alpha, \beta)$  in the case of axial symmetry can be found in Ref. [28], and the expressions used in the extension to the triaxial case will be included in a forthcoming publication.

The three projections of the IBM PESs on the  $(\beta, \gamma)$ ,  $(\alpha, \beta)$ , and  $(\gamma, \alpha)$  planes are shown in the second and fourth column of Fig. 1 for  $^{128}\text{Xe}$  and  $^{130}\text{Xe}$ , respectively. They are displayed next to the corresponding microscopic energy surfaces so that one can assess the mapping from the SCMF space of nucleon degrees of freedom to the boson space of the IBM.

We note that in a more traditional microscopic approach to large-amplitude collective motion, such as the collective Hamiltonian model [32, 48], the dynamics is

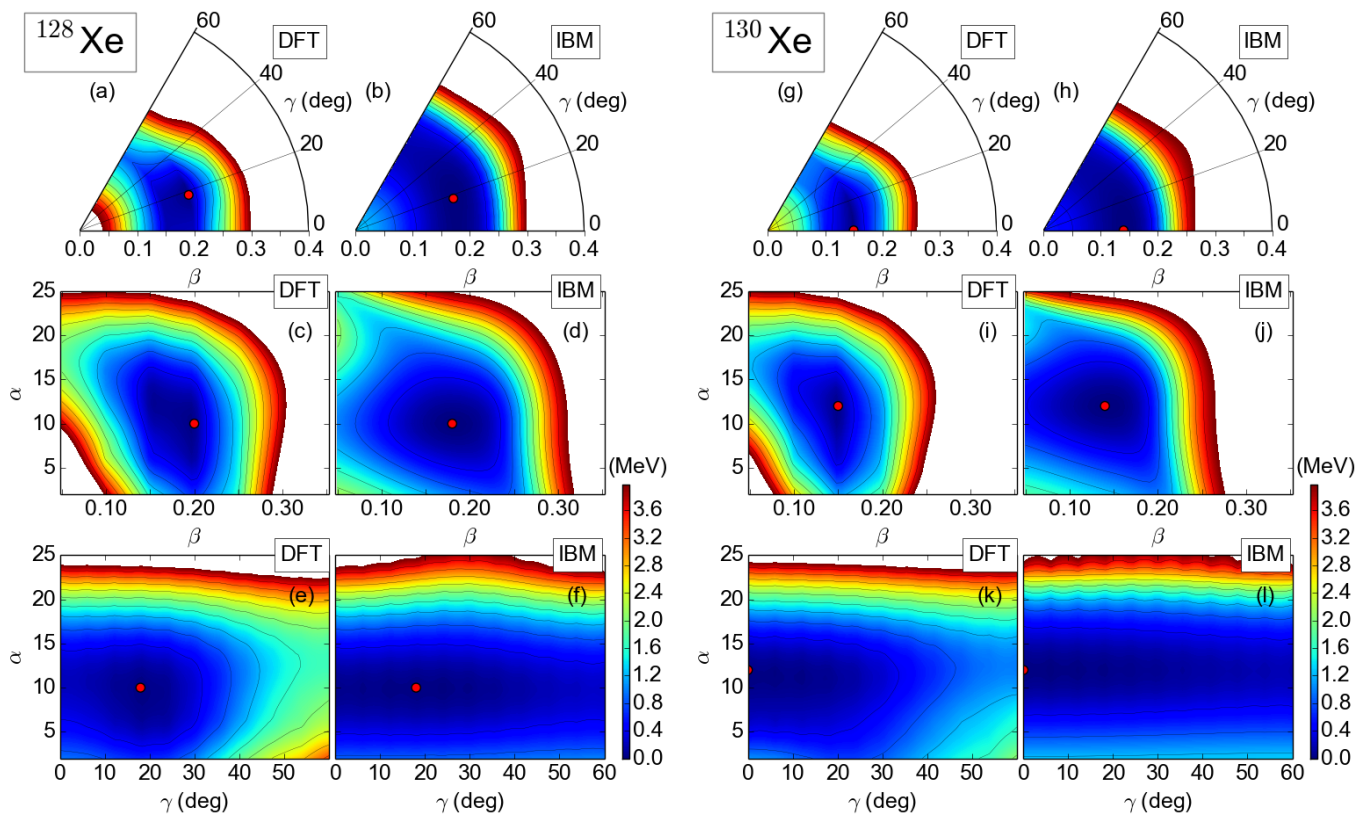


FIG. 1. Potential energy surfaces of  $^{128,130}\text{Xe}$  computed using the RMF+BCS model based on the functional PC-PK1 and a separable pairing interaction, and the interacting boson model (IBM) Hamiltonian determined by the microscopic SCMF energy maps (see text for the description). The 2D projections of the PESs are shown as functions of the axial quadrupole and triaxial  $(\beta, \gamma)$ , axial quadrupole and pairing  $(\beta, \alpha)$ , and triaxial quadrupole and pairing  $(\gamma, \alpha)$  deformations. The fixed values of  $\alpha = 10$  (12) in the  $(\beta, \gamma)$ ,  $\gamma = 18^\circ$  ( $0^\circ$ ) in the  $(\beta, \alpha)$ , and  $\beta = 0.2$  (0.15) in the  $(\gamma, \alpha)$  plot, correspond to the global minimum of the  $(\alpha, \beta, \gamma)$  PES of  $^{128}\text{Xe}$  ( $^{130}\text{Xe}$ ).

governed by the collective potential, the mass parameters, and moments of inertia, all defined as functions of the intrinsic deformation parameters. The single-nucleon wave functions, energies and occupation factors, generated from constrained SCMF calculations, provide the microscopic input for the parameters of the collective Hamiltonian. In the present approach, the collective dynamics is determined by the choice of the boson space ( $s$  and  $d$  bosons) and the IBM Hamiltonian that includes not only one-body, but also two-body and three-body boson interaction terms. Even though the parameters of this Hamiltonian do not explicitly depend on the intrinsic deformation parameters, the mapping of the entire SCMF energy surface on the expectation value of the IBM Hamiltonian in the boson condensate state, introduces an effective deformation dependence of the boson Hamiltonian. Of course, at very large deformations intruder orbitals become important, and the mapping to the limited boson space that corresponds to half the number of valence nucleons is too restrictive. However, in the vicinity of the equilibrium minimum the mapping is quite accurate (c.f. Fig. 1), and generally produces a bo-

son Hamiltonian that can describe low-energy excitation spectra at a quantitative level.

### III. EFFECT OF DYNAMICAL PAIRING AND TRIAXIAL DEFORMATION ON EXCITATION SPECTRA

Having determined the parameters of the IBM Hamiltonian, we next consider spectroscopic properties and discuss the importance of simultaneously incorporating dynamical pairing and triaxial degrees of freedom in the model space. As already shown in Ref. [28] for axially symmetric calculations of  $^{122}\text{Xe}$  and rare-earth  $N = 92$  isotones, the coupling between shape and pairing collective degrees of freedom has hardly any effect on states of the yrast band, either on excitation energies or transition rates. In contrast, the inclusion of dynamical pairing significantly lowers the energies of bands based on excited  $0^+$  states. Figure 2 displays the excitation energies of the second, third, and fourth  $0^+$  states in  $^{128}\text{Xe}$  and  $^{130}\text{Xe}$ . We plot the energies calculated with the IBM in-

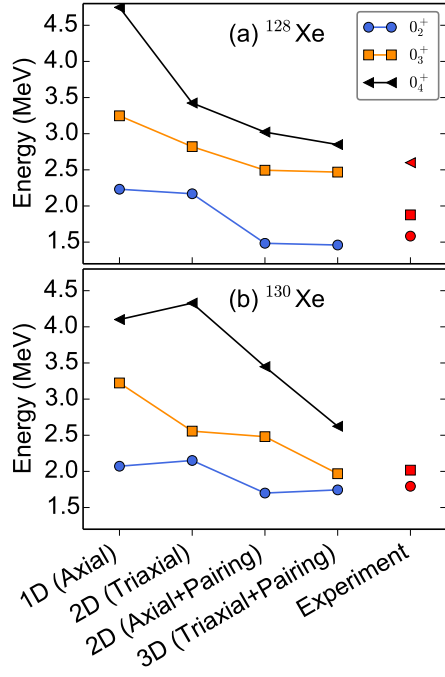


FIG. 2. Excitation energies of the second, third, and fourth  $0^+$  states in  $^{128}\text{Xe}$  and  $^{130}\text{Xe}$ . Results obtained with the IBM including 1D axial quadrupole ( $\beta$ ), 2D triaxial quadrupole ( $\beta, \gamma$ ) and pairing plus axial quadrupole ( $\alpha, \beta$ ), and 3D pairing plus triaxial quadrupole ( $\alpha, \beta, \gamma$ ) degrees of freedom are compared with experimental values (filled red symbols on the right-hand side of each panel).

cluding 1D axial quadrupole ( $\beta$ ), 2D triaxial quadrupole ( $\beta, \gamma$ ) and pairing plus axial quadrupole ( $\alpha, \beta$ ) and, finally, 3D pairing plus triaxial quadrupole ( $\alpha, \beta, \gamma$ ) degrees of freedom. The lines are a guide to the eye, and the experimental values are denoted by filled red symbols on the right-hand side of each panel. Because of configuration mixing it is not possible to uniquely separate the effects of triaxial deformations and pairing vibrations on each  $0^+$  state. However, the inclusion of these degrees of freedom generally lowers the  $0^+$  states, bringing the excitation energies in a quantitatively better agreement with experiment. In the particular examples considered here, it appears that the energies of  $0_2^+$  are not sensitive to the inclusion of triaxial deformations, whereas both  $\gamma$ -deformation and dynamical pairing have an effect on the excitation energies of  $0_3^+$  and  $0_4^+$ . One should keep in mind that these model calculations are performed in the collective monopole and quadrupole boson space. In actual nuclei, however, two- or four-quasiparticle states play a role at higher excitation energies, e.g. above  $\approx 3$  MeV, but these degrees of freedom are not included in our model space. Even though a mixing with these states would, of course, affect the calculated excitation energies, the qualitative effect of dynamical pairing would still be the lowering of excited  $0^+$  states.

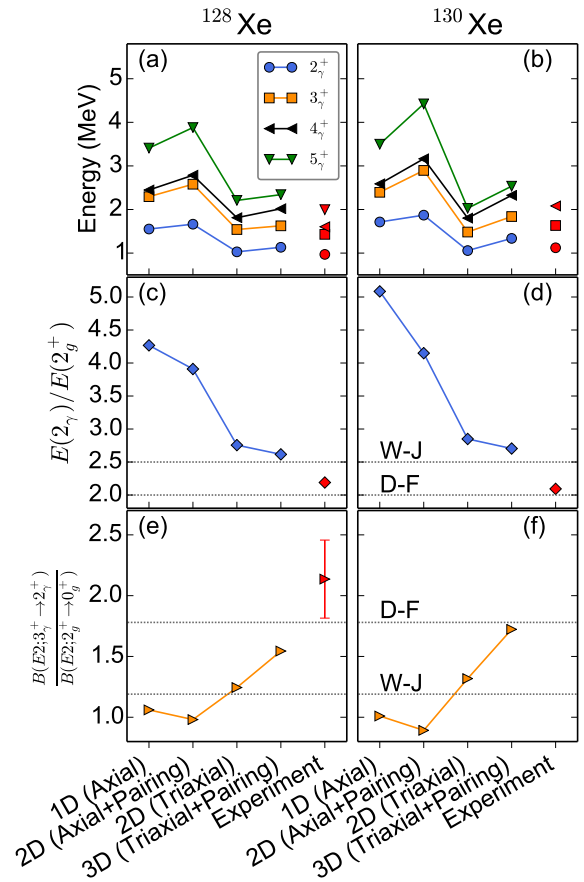


FIG. 3. Excitation spectra of the states belonging to the  $\gamma$ -band (a,b), the energy ratio  $E_{2\gamma} = E(2_\gamma^+)/E(2_g^+)$  (c,d), and the ratio  $R_{3\gamma} = B(E2; 3_\gamma^+ \rightarrow 2_\gamma^+)/B(E2; 2_g^+ \rightarrow 0_g^+)$  (e,f), obtained by four different IBM calculations of  $^{128}\text{Xe}$  and  $^{130}\text{Xe}$ : axially deformed, axially deformed + dynamical pairing, triaxially deformed, and triaxially deformed + dynamical pairing. In panels (c,d,e,f), the values predicted by the triaxial rotor model of Davydov and Filippov (D-F) at  $\gamma = 30^\circ$  [3] ( $E_{2\gamma} = 2.00$  and  $R_{3\gamma} = 1.78$ ), and by the  $\gamma$ -unstable-rotor model of Wilets and Jean (W-J) or  $O(6)$  symmetry [4, 49] ( $E_{2\gamma} = 2.50$  and  $R_{3\gamma} = 1.19$ ) are also indicated by dotted horizontal lines. Available experimental values from Refs. [50–52] are shown by filled red symbols on the right-hand side of each panel.

A similar analysis is performed for the excitation energies of the members of the  $\gamma$ -bands of  $^{128}\text{Xe}$  and  $^{130}\text{Xe}$ , and illustrated in the top panels of Fig. 3. As one would expect, in this case the effect of the inclusion of triaxial deformations is important to reproduce the experimental excitation energies of the members of the  $\gamma$  band. One notes, however, that the coupling with pairing vibrations increases the excitation energy of the  $\gamma$ -band. This is somewhat at variance with the experimental data, the deviation attributed to the level repulsion due to the configuration mixing between the subspaces (1) of the IBM.

We have further analyzed two quantities that char-

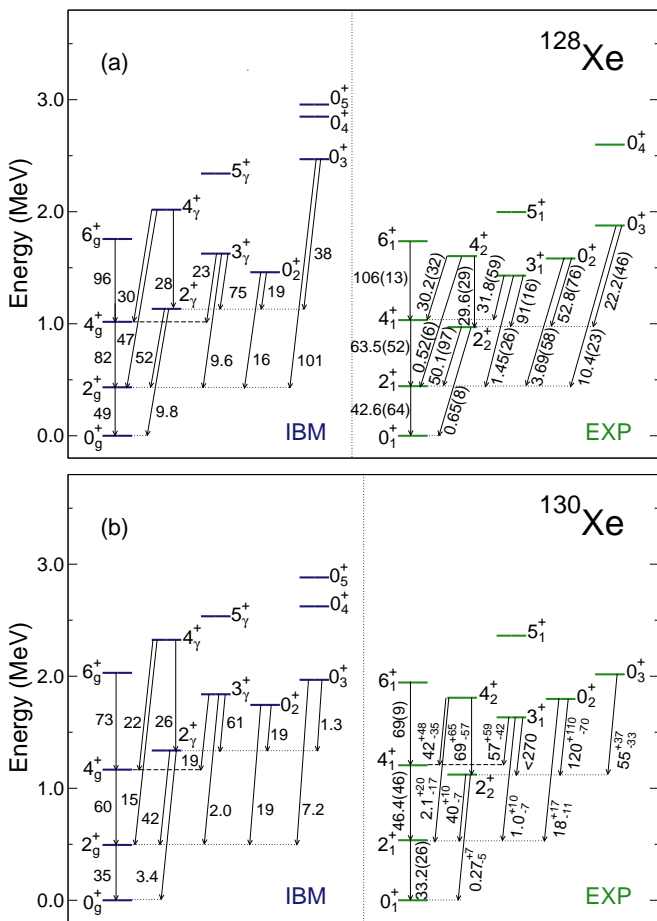


FIG. 4. Low-energy excitation spectra of  $^{128,130}\text{Xe}$  obtained with the IBM that includes dynamical pairing and triaxial deformation degrees of freedom. The levels are grouped into bands according to the dominant transitions, and the  $B(E2)$  values are in Weisskopf units. The results of model calculation are compared to the corresponding experimental energy spectra [50–52].

acterize the level of  $\gamma$ -softness. The limiting cases are described by two geometrical models: the rigid-triaxial-rotor model of Davydov and Filippov (D-F), and the  $\gamma$ -unstable rotor model of Wilets and Jean (W-J). The latter is equivalent to the  $O(6)$  dynamical symmetry of the IBM [49, 53]. To distinguish between rigidity and softness in  $\gamma$ , we consider the ratios  $E_{2\gamma} = E(2_{\gamma}^+)/E(2_g^+)$  and  $R_{3\gamma} = B(E2; 3_{\gamma}^+ \rightarrow 2_{\gamma}^+)/B(E2; 2_g^+ \rightarrow 0_g^+)$ . They are plotted in the middle and lower rows of Fig. 3, respectively. Note that for the  $B(E2)$  values, because three-body boson terms are included in the Hamiltonian, calculations with triaxial degree of freedom should in principle contain higher-order terms in the  $E2$  transition operator [40]. Both calculated quantities exhibit a pronounced dependence on the triaxial degree of freedom. The results of the full calculation for  $E_{2\gamma}$  are closer to the W-J limit, while the  $R_{3\gamma}$  values trend towards the D-F limit.

Finally, we demonstrate that the model is also capable of describing detailed structure properties of  $\gamma$ -soft nuclei. In Fig. 4 the low-energy excitation spectra of  $^{128}\text{Xe}$  and  $^{130}\text{Xe}$ , obtained with the IBM that includes the dynamical pairing and triaxial deformation degrees of freedom, are compared to the corresponding experimental energy spectra [50–52]. On closer inspection it is seen that the present IBM calculation reproduces the available low-energy data. Characteristic features of  $\gamma$ -soft nuclei emerge in the calculated excitation spectra: the low energy of the band-head of  $\gamma$  band ( $2_{\gamma}^+$ ), the level spacing between the states of the  $\gamma$  band, and the excitation energy of the  $0_2^+$  state relative to the  $\gamma$  band.

For  $^{128}\text{Xe}$  the present calculation predicts the  $\gamma$ -band at somewhat higher excitation energy compared to its experimental counterpart. The  $0_2^+$  state is slightly lower than the corresponding experimental level, while the calculated  $0_3^+$  is at considerably higher excitation energy. The  $0_2^+$  wave function is dominated by components that are almost equally distributed between the  $[n_0 - 1]$  and  $[n_0 + 1]$  subspaces (more than 90%), that is, the structure corresponds to a pairing vibrational state. In contrast, the boson distribution of  $0_3^+$  is very similar to that of the ground-state band, with predominant components in the  $[n_0]$  subspace. This is reflected in the strong  $E2$  transition to the state  $2_1^+$  ( $2_g^+$ ), with a  $B(E2)$  value an order of magnitude larger than in experiment. The observed  $E2$  transition strengths [50, 51] are, in general, reproduced by the model calculation, except for the weak transition  $4_2^+ \rightarrow 2_1^+$ . The calculated  $B(E2)$  value is, in fact, larger than that of the corresponding  $4_{\gamma}^+ \rightarrow 4_g^+$  transition, which reproduces the experimental value.

The calculated spectrum of  $^{130}\text{Xe}$  reproduces the data equally well and, in fact, the excitation energies of the states  $0_2^+$  and  $0_3^+$  are in better agreement with experiment compared to the previous case. Here both  $0_2^+$  and  $0_3^+$  exhibit a structure that can be interpreted as pairing vibrations, while the largest component of the wave function of  $0_4^+$  is that of the  $[n_0]$  subspace. Just as in the case of  $^{128}\text{Xe}$ , the  $\gamma$ -band is calculated at somewhat higher excitation energy with respect to experiment. The predicted transition rates are consistent with the available data even though, except for yrast band, the latter are dominated by large error bars.

#### IV. CONCLUSION

Based on self-consistent mean-field calculations of deformation energy surfaces, and the framework of the interacting boson approximation, a new method has been developed that allows for the coupling between pairing and triaxial ( $\beta, \gamma$ ) shape degrees of freedom. In addition to quadrupole shape vibrations and rotations, the explicit coupling to pairing vibrations is taken into account by a boson-number non-conserving IBM Hamiltonian. The parameters of the Hamiltonian are specified by SCMF calculations for a specific choice of a universal energy den-

sity functional and pairing interaction, with constraints on quadrupole shape and pairing intrinsic deformations. The illustrative calculation of low-energy excitation spectra of  $^{128}\text{Xe}$  and  $^{130}\text{Xe}$  indicates the importance of the dynamical pairing degree of freedom, especially for low-energy  $0^+$  excited states and bands based on them. The findings of the present study will pave the way for more detailed explorations of pairing vibrations in various regions of  $\gamma$ -soft and triaxial nuclei.

## ACKNOWLEDGMENTS

This work has been supported by the Tenure Track Pilot Programme of the Croatian Science Foundation and the École Polytechnique Fédérale de Lausanne, and the Project TTP-2018-07-3554 Exotic Nuclear Structure and Dynamics, with funds of the Croatian-Swiss Research Programme. It has also been supported in part by the QuantiXLie Centre of Excellence, a project co-financed by the Croatian Government and European Union through the European Regional Development Fund - the Competitiveness and Cohesion Operational Programme (KK.01.1.1.01). The author Z.P.L. acknowledges support by the NSFC under Grant No. 11875225. The author J.X. acknowledges support by the NSFC under Grants No. 12005109 and No. 11765015.

- 
- [1] A. Bohr and B. R. Mottelson, *Nuclear Structure*, Vol. II (Benjamin, New York, USA, 1975).
- [2] P. Ring and P. Schuck, *The Nuclear Many-Body Problem* (Springer-Verlag, Berlin, 1980).
- [3] A. S. Davydov and G. F. Filippov, *Nucl. Phys.* **8**, 237 (1958).
- [4] L. Wilets and M. Jean, *Phys. Rev.* **102**, 788 (1956).
- [5] N. V. Zamfir and R. F. Casten, *Phys. Lett. B* **260**, 265 (1991).
- [6] R. F. Casten, *Nuclear Structure from a Simple Perspective* (Oxford University Press, Oxford, England, 2000).
- [7] E. A. McCutchan, D. Bonatsos, N. V. Zamfir, and R. F. Casten, *Phys. Rev. C* **76**, 024306 (2007).
- [8] K. Nomura, N. Shimizu, D. Vretenar, T. Nikšić, and T. Otsuka, *Phys. Rev. Lett.* **108**, 132501 (2012).
- [9] T. Nikšić, P. Marević, and D. Vretenar, *Phys. Rev. C* **89**, 044325 (2014).
- [10] N. L. Vaquero, T. R. Rodríguez, and J. L. Egidio, *Phys. Rev. Lett.* **111**, 142501 (2013).
- [11] S. A. Giuliani, L. M. Robledo, and R. Rodríguez-Guzmán, *Phys. Rev. C* **90**, 054311 (2014).
- [12] J. Zhao, B.-N. Lu, T. Nikšić, D. Vretenar, and S.-G. Zhou, *Phys. Rev. C* **93**, 044315 (2016).
- [13] N. Schunck and L. M. Robledo, *Rep. Prog. Phys.* **79**, 116301 (2016).
- [14] R. Bernard, S. A. Giuliani, and L. M. Robledo, *Phys. Rev. C* **99**, 064301 (2019).
- [15] D. R. Bès, *Nucl. Phys.* **49**, 544 (1963).
- [16] D. R. Bès and C. Yi-Chung, *Nucl. Phys.* **86**, 581 (1966).
- [17] R. F. Casten, E. R. Flynn, J. D. Garrett, O. Hansen, T. J. Mulligan, D. R. Bess, R. A. Broglia, and B. Nilsson, *Phys. Lett. B* **40**, 333 (1972).
- [18] I. Ragnarsson and R. A. Broglia, *Nucl. Phys. A* **263**, 315 (1976).
- [19] D. R. Bès and R. A. Broglia, *Nucl. Phys.* **80**, 289 (1966).
- [20] D. R. Bès, R. A. Broglia, R. P. J. Perazzo, and K. Kumar, *Nucl. Phys. A* **143**, 1 (1970).
- [21] D. R. Bès, R. A. Broglia, and B. Nilsson, *Phys. Lett. B* **40**, 338 (1972).
- [22] D. M. Brink and R. A. Broglia, *Nuclear superfluidity: pairing in finite systems* (Cambridge University Press, Cambridge, 2005).
- [23] P. E. Garrett, *J. Phys. G: Nucl. Part. Phys.* **43**, 084002 (2016).
- [24] L. Próchniak, K. Zajęc, K. Pomorski, S. G. Rohoziński, and J. Srebrny, *Nucl. Phys. A* **648**, 181 (1999).
- [25] J. Srebrny, T. Czosnyka, C. Droste, S. G. Rohoziński, L. Próchniak, K. Zajęc, K. Pomorski, D. Cline, C. Y. Wu, A. Bäcklin, L. Hasselgren, R. M. Diamond, D. Habs, H. J. Körner, F. S. Stephens, C. Baktash, and R. P. Kosteci, *Nucl. Phys. A* **766**, 25 (2006).
- [26] L. Próchniak, *Int. J. Mod. Phys. E* **16**, 352 (2007).
- [27] J. Xiang, Z. P. Li, T. Nikšić, D. Vretenar, and W. H. Long, *Phys. Rev. C* **101**, 064301 (2020).
- [28] K. Nomura, D. Vretenar, Z. P. Li, and J. Xiang, *Phys. Rev. C* **102**, 054313 (2020).
- [29] K. Heyde and J. L. Wood, *Rev. Mod. Phys.* **83**, 1467 (2011).
- [30] M. Bender, P.-H. Heenen, and P.-G. Reinhard, *Rev. Mod. Phys.* **75**, 121 (2003).
- [31] D. Vretenar, A. Afanasjev, G. Lalazissis, and P. Ring, *Phys. Rep.* **409**, 101 (2005).
- [32] T. Nikšić, D. Vretenar, and P. Ring, *Prog. Part. Nucl. Phys.* **66**, 519 (2011).
- [33] L. M. Robledo, T. R. Rodríguez, and R. R. Rodríguez-Guzmán, *J. Phys. G: Nucl. Part. Phys.* **46**, 013001 (2019).
- [34] J. Xiang, Z. P. Li, Z. X. Li, J. M. Yao, and J. Meng, *Nucl. Phys. A* **873**, 1 (2012).
- [35] P. W. Zhao, Z. P. Li, J. M. Yao, and J. Meng, *Phys. Rev. C* **82**, 054319 (2010).
- [36] Y. Tian, Z. Y. Ma, and P. Ring, *Phys. Lett. B* **676**, 44 (2009).
- [37] K. Nomura, N. Shimizu, and T. Otsuka, *Phys. Rev. Lett.* **101**, 142501 (2008).
- [38] T. Otsuka, A. Arima, and F. Iachello, *Nucl. Phys. A* **309**, 1 (1978).
- [39] P. Van Isacker and J.-Q. Chen, *Phys. Rev. C* **24**, 684 (1981).
- [40] K. Heyde, P. Van Isacker, M. Waroquier, and J. Moreau, *Phys. Rev. C* **29**, 1420 (1984).
- [41] R. Casten, P. von Brentano, K. Heyde, P. Van Isacker, and J. Jolie, *Nucl. Phys. A* **439**, 289 (1985).

- [42] J. N. Ginocchio and M. W. Kirson, Nucl. Phys. A **350**, 31 (1980).
- [43] A. E. L. Dieperink, O. Scholten, and F. Iachello, Phys. Rev. Lett. **44**, 1747 (1980).
- [44] A. Frank, P. Van Isacker, and C. E. Vargas, Phys. Rev. C **69**, 034323 (2004).
- [45] K. Nomura, T. Otsuka, N. Shimizu, and L. Guo, Phys. Rev. C **83**, 041302 (2011).
- [46] D. R. Inglis, Phys. Rev. **103**, 1786 (1956).
- [47] S. T. Beliaev, Nucl. Phys. **24**, 322 (1961).
- [48] L. Próchniak and S. G. Rohoziński, J. Phys. G: Nucl. Part. Phys. **36**, 123101 (2009).
- [49] F. Iachello and A. Arima, *The interacting boson model* (Cambridge University Press, Cambridge, 1987).
- [50] Brookhaven National Nuclear Data Center, <http://www.nndc.bnl.gov>.
- [51] L. Coquard, N. Pietralla, T. Ahn, G. Rainovski, L. Bettermann, M. P. Carpenter, R. V. F. Janssens, J. Leske, C. J. Lister, O. Möller, W. Rother, V. Werner, and S. Zhu, Phys. Rev. C **80**, 061304 (2009).
- [52] E. E. Peters, T. J. Ross, S. F. Ashley, A. Chakraborty, B. P. Crider, M. D. Hennek, S. H. Liu, M. T. McEllistrem, S. Mukhopadhyay, F. M. Prados-Estévez, A. P. D. Ramirez, J. S. Thrasher, and S. W. Yates, Phys. Rev. C **94**, 024313 (2016).
- [53] A. Arima and F. Iachello, Ann. Phys. **123**, 468 (1979).